

Pd/PVDF thin film hydrogen sensor system based on photopyroelectric purely-thermal-wave interference

Chinhua Wang, Andreas Mandelis^{*}, Jose A. Garcia

Photothermal and Optoelectronic Diagnostics Laboratories, Department of Mechanical and Industrial Engineering, University of Toronto, 5 King's College Road, Toronto, Ontario, Canada M5S 3G8

Accepted 9 August 1999

Abstract

A novel sensitive solid-state sensor system for trace hydrogen gas detection has been developed as a next generation device to earlier photopyroelectric (PPE) hydrogen sensors. The basic principle of the sensor is based on the technique of PPE purely-thermal-wave interferometry recently developed in this Laboratory. The active element of the sensor is a thin polyvinylidene fluoride (PVDF) pyroelectric film, sputter-coated with Pd on one surface and with a Ni–Al alloy electrode on the other surface. Unlike the conventional PPE hydrogen sensors, this new sensor produces a coherent differential PPE signal in a single detector, rather than using two detectors (one active, the other reference) and complicated electronics. The measurement results show that the signal noise level, the detectivity and the signal dynamic range are improved by more than one order of magnitude compared with the conventional single-beam method. The operating characteristics have been examined for three different thicknesses of Pd coating on the same thickness PVDF-film detector. The signal generating mechanism, attributed to the change of the optical absorptance of the Pd coating when exposed to hydrogen, and/or the shift in the Pd work function, is also discussed. © 1999 Elsevier Science S.A. All rights reserved.

Keywords: Thermal-wave; Destructive interferometry; Photopyroelectric thin film; Hydrogen sensor

1. Introduction

In the last decade, hydrogen gas has become a technologically important substance due to the widespread use of hydrogen in a variety of industrial fields, with the consequence that fast, in situ monitoring of trace amounts of hydrogen is becoming increasingly important. Therefore, a considerable research effort has been directed toward the development of hydrogen gas sensors [1–14]. Among the large variety of hydrogen gas sensors, most are based on electronic devices and use palladium as the active membrane. Lundstrom et al. reported on Pd-gate MOS transistors and Pd-gate metal–insulator–semiconductor (MIS) sensors [2,3]. Steele and MacIver [4], and D'Amico et al. [5], showed that a Pd–CdS and a Pd–insulator Schottky barrier diode, respectively, exhibited a response to hydrogen. The double metal-gate MISFET [6] and the insulator-gate field-effect transistor (IGFET) [7] appear to have been successful as hydrogen sensors as well. Furthermore, a

variety of other hydrogen sensors have been developed: a surface acoustic wave (SAW) sensor [1,8], an optical fiber sensor [1,9], and an optical interferometric sensor [1,10]. To date, work in our laboratory has been directed toward the fabrication of Pd-coated polyvinylidene (di)fluoride (Pd-PVDF) thin film photopyroelectric (PPE) sensors [11–15]. This kind of sensor has advantages over the use of a glass substrate [16–18] in terms of fabrication simplicity and peel-off or blister avoidance, presumably due to the accommodation/matching by the PVDF polymer substrate of the Pd-film lattice-constant expansion. Mandelis and Christofides detected down to 0.075% hydrogen concentration in a flowing H₂ + N₂ mixture by employing two detectors (one active and one reference) and two-signal processing electronics [11]. Since then, efforts have been made to simplify the detection system by employing either a purely optical method [12,13] or by use of a single-detector method [15]. The detectivity, signal quality, and signal dynamic range, however, are compromised due to the large baseline signal, which requires the use of low instrumental sensitivity [12,13,15]. In addition, noise is introduced through the intensity fluctuation of the incident light. In

^{*} Corresponding author. Tel.: +1-416-978-5106; fax: +1-416-266-7867; e-mail: mandelis@mie.utoronto.ca

this paper, a novel Pd-PVDF PPE hydrogen sensor, based on the very recently developed purely-thermal-wave interferometric technique [19,20], is described. A fully destructive thermal-wave interference pattern within the PVDF detector makes it possible to implement a simple, differential and high-sensitivity measurement using a single PVDF thin film.

2. Experimental arrangement and sensor principle

A schematic representation of the experimental arrangement is shown in Fig. 1(a). The experimental setup consists of four subsystems: gas supply; test cell; signal generation; and data acquisition. The gas-supply component mixes hydrogen and nitrogen in a homogeneous flow. The flow rate of each gas can be adjusted and stabilized before the mixture is directed into the test cell. High purity hydrogen (99.999%), zero grade nitrogen (99.9975%) and 1.07% hydrogen in nitrogen by volume from Matheson Gas Products were used to obtain the desired hydrogen concentrations. The test cell was made of aluminum with an inlet and outlet for the ambient gas, two optical windows for the incident light to enter from opposite sides of

the active PVDF element, and had a volume of ~ 150 ml. The test cell contained a Pd–PVDF–NiAl thin film, which was mounted on an aluminum base. Three different Pd–PVDF–NiAl thin films were used: they had the same thickness of the PVDF layer (52 μm), and the same thickness of the NiAl coating (15 nm Ni + 35 nm Al) on one surface. The opposite surface was coated with three different Pd thicknesses (6.5, 25.6, and 53.4 nm) to optimize the sensor operating behavior. A cellular plastic plate was placed in front of the gas inlet to further disperse the gas into a homogeneous stream before it reaches the thin film. Special care was also taken to introduce the gas flow parallel to the surfaces of the Pd–PVDF–NiAl film so that both surfaces could be exposed to the gas mixture under the same conditions, which reduces gas flow anisotropy bias on either surface of the sensor. A detailed schematic representation of the test cell is shown in Fig. 1(b). Two laser beams (intensities I_1 and I_2), were obtained from a single He–Ne laser beam (15 mW) by using a beam splitter. They were modulated with a mechanical chopper at the same angular frequency (ω) and with a fixed, adjustable phase shift ($\Delta\varphi$). One beam was incident onto the front (Pd coating) and the other beam was directed to the rear (NiAl-coated) surface of the PVDF detector from opposite directions. Different ratios of the two incident intensities and the phase shift between the two beams yield different thermal-wave interference patterns inside the PVDF detector [19,20]. A fully destructive interferometric pattern is produced when the intensities of the two beams are identical and the phase shift between them is 180° . This destructive operating mode of the PVDF detector yields a sensitive coherent differential method to detect minute changes in the PPE output signal, using a single transducer. It is well known that Pd metal interacts reversibly with hydrogen gas to form a hydride. Associated with these compositional changes are changes in the optical properties (reflectance and absorptance), and in electronic properties (electrostatic charge distribution) in the palladium [9,12–14,21–23]. Therefore, a minute change in the PPE output is caused by the change in optical absorptivity and electrostatics of the Pd coating on one surface, while the properties of NiAl coating on the other surface remain unchanged. The output PPE signal from the detector is then fed to a lock-in amplifier. The data acquisition was facilitated by a personal computer through a serial port.

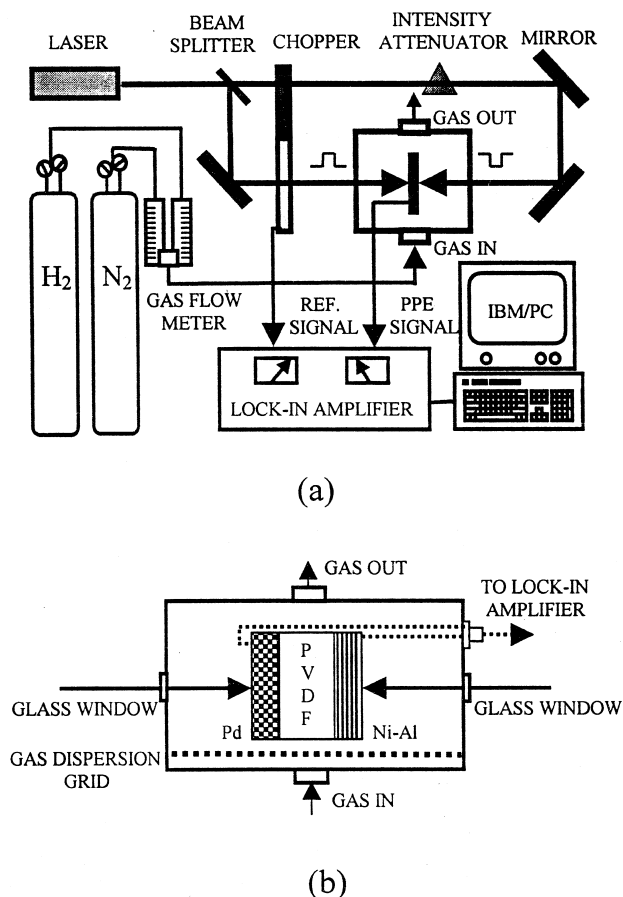


Fig. 1. (a) Schematic representation of the PPE interferometric sensor setup; (b) Cross-sectional detail of the test cell.

3. PPE signal generation phenomenology and device physics

Poled PVDF thin films (β phase) are known to exhibit strong pyroelectricity; i.e., a potential difference is generated in the direction of poling between the two metallized electrode surfaces which sandwich the pyroelectric film when a temperature change is induced within the pyroelec-

tric layer [24]. The physical mechanism of sensor operation is known to be threefold: One component of the PPE signal is due to the optical absorptance and reflectivity asymmetry, which is established between the front Pd film and the back NiAl electrode following exposure to hydrogen gas. This asymmetry results in different optical powers being absorbed between the front and back surfaces of the PVDF sensor. Upon optical-to-thermal power conversion at each metallic layer, non-equal thermal-wave fields are produced inside the bulk of the sensor. The destructive interferometric nature of the superposition thermal-wave field yields a non-zero PPE signal component directly proportional to the difference in the PVDF thickness-integrated thermal-wave distributions in the sensor bulk. These can be traced back to differences in absorptances (or reflectivities) between the two metallic layers/electrodes. Secondly, the change of ambient gas thermophysical properties (thermal diffusivity and conductivity) upon introduction of hydrogen gas, affects the boundary conditions of the thermal-wave generated optically inside the bulk of the PVDF film and contributes a PPE signal component. In the case of the replacement of air by hydrogen ambient in the cell, the thermophysical property change can be significant due to the much higher conductivity and diffusivity of hydrogen gas [14]. The final component is due to unequal work-function changes between these two metallic layers upon exposure to hydrogen.

The first two components are coupled thermal-related contributions from the temperature change inside the PVDF layer in the configuration of Fig. (1b). They can be calculated by solving coupled one-dimensional heat diffusion equations subject to appropriate boundary conditions. For these calculations, the basic geometry of the PVDF detector is shown in Fig. 2. The PVDF thin film (P) of thickness d with Pd coating on one surface and NiAl coating on the other surface is surrounded by semi-infinite regions of gas (g_1 and g_2) on both sides. Considering the large surface absorptance of the metallic coatings and the

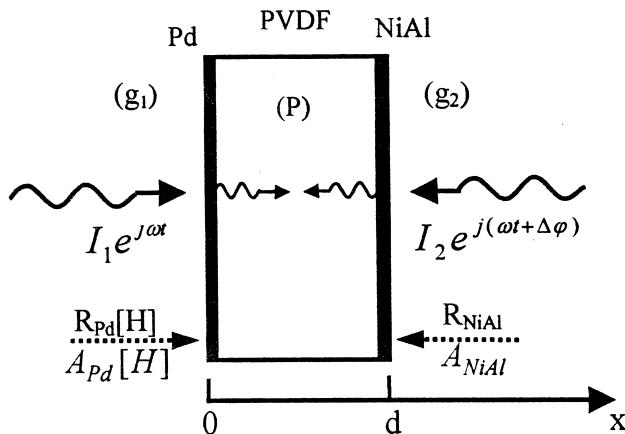


Fig. 2. Cross-sectional geometry of the Pd–PVDF–NiAl sensor for device physics analysis. $R_{Pd}[H]$, $A_{Pd}[H]$; and R_{NiAl} , A_{NiAl} are surface reflectivities and absorptances of the Pd and NiAl coating, respectively.

essentially transparent nature of PVDF at the He–Ne laser excitation wavelength [24], the thermal source within the PVDF bulk due to partially transmitted light through the metallic coatings is neglected for simplicity. In the most general case considered here, the transmitted fraction of the front beam through the Pd coating and across the PVDF bulk is correspondingly absorbed by the NiAl coating. A similar process is assumed regarding the back beam. All the higher-order interreflections are neglected. We define k_i ($i = g, p$) to be the thermal conductivity of medium i . $A_{Pd}[H]$, $R_{Pd}[H]$ and A_{NiAl} , R_{NiAl} are the optical absorptance and the optical reflectivity of the Pd coating and the NiAl coating, respectively. The absorptance $A_{Pd}[H]$ and reflectivity $R_{Pd}[H]$ have been expressed as functions of the concentration $[H]$ in the Pd film [9,12–14,21–23]. This concentration is a thermodynamic equilibrium function of the ambient H_2 gas concentration. Therefore, the appropriate heat diffusion equations have the form:

$$\frac{d^2 T_i(x, \omega)}{dx^2} - \sigma_i^2 T_i(x, \omega) = 0, \quad i = 1, 2, \quad (1)$$

p for regions g_1 , g_2 , and P, respectively.

Here $\sigma_i = (1 + j)\sqrt{\omega/2\alpha_i}$ is the complex wave number for the i th medium ($j^2 = -1$), and α_i is the thermal diffusivity of the medium. Applying boundary conditions of (a) continuity of the temperature and (b) conservation of the heat flux at $x = 0$ and $x = d$ results in the following equations:

$$T_1(0, \omega) = T_p(0, \omega) \quad (2)$$

$$T_p(d, \omega) = T_2(d, \omega) \quad (3)$$

$$k_g \frac{\partial T_1(0, \omega)}{\partial x} - k_p \frac{\partial T_p(0, \omega)}{\partial x} = I_1 A_{Pd}[H] + I_2 e^{j\Delta\phi} A_{Pd}[H] (1 - R_{NiAl} - A_{NiAl}) \quad (4)$$

$$k_p \frac{\partial T_p(d, \omega)}{\partial x} - k_g \frac{\partial T_2(d, \omega)}{\partial x} = I_2 e^{j\Delta\phi} A_{NiAl} + I_1 A_{NiAl} (1 - R_{Pd}[H] - A_{Pd}[H]) \quad (5)$$

where the right-hand sides of Eqs. (4) and (5) represent the aforementioned optical absorption contributions within the two quasi-transparent metallic coating surfaces. Therefore, the PPE signal component due to thermal-wave generation across the PVDF bulk and due to changes in the boundary conditions of temperature and heat flux at the sensor–gas interface, is proportional to the thickness-averaged temperature $\langle T_p \rangle$ of the PVDF film and can be obtained by solving Eq. (1) [25]:

$$V_i(\omega) = Q(\omega) \langle T_p(x, \omega) \rangle = \frac{Q(\omega)}{d} \left[C_1 \int_0^d e^{-\sigma_p x} dx + C_2 \int_0^d e^{\sigma_p x} dx \right] \quad (6)$$

where $Q(\omega)$ is an instrumental factor related to the transfer function of the detector and its associated electronics; C_1 and C_2 are integration constants, determined from the boundary conditions, Eqs. (2)–(5). Solution of the boundary-value problem of Eqs. (1)–(6) gives the PPE thermal-wave-originating signal V_t

$$V_t(\omega, [H]) = S(\omega, [H]) \{ I_1 [A_{Pd}[H] + A_{NiAl}(1 - R_{Pd}[H] - A_{Pd}[H])] + I_2 e^{j\Delta\varphi} [A_{NiAl} + A_{Pd}[H](1 - R_{NiAl} - A_{NiAl})] \} \quad (7)$$

where

$$\begin{aligned} S(\omega, [H]) &\cong S(\omega) \\ &= Q(\omega) \frac{(e^{\sigma_p d} - 1 + \gamma_{gp}[H] - \gamma_{gp}[H]e^{-\sigma_p d})}{k_p \sigma_p^2 (1 + b_{gp}[H]) (e^{\sigma_p d} - \gamma_{gp}^2[H]e^{-\sigma_p d})} \end{aligned} \quad (8)$$

and $b_{gp}[H] = e_g[H]/e_p$, $\gamma_{gp}[H] = (1 - b_{gp}[H])/(1 + b_{gp}[H])$. These factors incorporate the effects on the thermal-wave PPE signal of changed boundary conditions in the presence of hydrogen gas. Here e_i is the thermal effusivity of material (or gas) (i). Once a PVDF thin film is chosen, the PVDF-related parameters of the active element and the detection system are fixed constants as hydrogen concentration varies. For the air–PVDF and hydrogen–PVDF system under consideration, $b_{gp}[H] \ll 1$, and thus the hydrogen dependence of the thermal parameters is neglected when compared with the contributions from the change of optical absorptance and reflectivity of Pd coating, i.e., $S(\omega, [H])$ is considered as being independent of H_2 concentration, $S(\omega)$.

It can be seen from Eq. (7) that the PPE output is a function of relative intensities (I_1 and I_2), modulation frequency (ω) and phase shift ($\Delta\varphi$) of the two incident laser beams, as well as of the reflectivities of the two coated surfaces of the PVDF film. As already mentioned, the PPE output can be easily adjusted to zero by means of changing the relative intensities and the phase shift of the two beams prior to introducing H_2 gas into the test cell. As a result of this operation, we can write that, initially

$$\begin{aligned} I_1 [A_{Pd}[0] + A_{NiAl}(1 - R_{Pd}[0] - A_{Pd}[0])] \\ = I_2 [A_{NiAl} + A_{Pd}[0](1 - R_{NiAl} - A_{NiAl})] \end{aligned} \quad (9a)$$

and

$$\Delta\varphi = 180^\circ \quad (9b)$$

where $R_{Pd}[0]$, $A_{Pd}[0]$ represent the reflectivity and absorptance of the Pd coating at zero $[H_2]$ concentration. Upon introduction of hydrogen into the test cell, a non-zero PPE signal appears because hydrogen is adsorbed on and absorbed in, the palladium film. In doing so, it subsequently changes the surface reflectance and absorptance of the Pd

coating, while R_{NiAl} remains unaltered. Therefore, the differential thermal PPE signal is given by the relation

$$\begin{aligned} V_t(\omega, [H]) = S(\omega) \{ I_1 [A_{Pd}[H] + A_{NiAl}(1 - R_{Pd}[H] \\ - A_{Pd}[H])] - I_2 [A_{NiAl} + A_{Pd}[H] \\ \times (1 - R_{NiAl} - A_{NiAl})] \} \end{aligned} \quad (10)$$

By substituting the relationship Eq. (9a) into Eq. (10), we obtain

$$\begin{aligned} V_t(\omega, [H]) &= \frac{S(\omega)}{[A_{NiAl} + A_{Pd}[0](1 - R_{NiAl} - A_{NiAl})]} \\ &\times I_1 \{ A_{NiAl}^2 (R_{Pd}[0] - R_{Pd}[H]) \\ &- A_{NiAl} R_{NiAl} (A_{Pd}[0] - A_{Pd}[H]) \\ &+ A_{NiAl} (1 - R_{NiAl} - A_{NiAl}) (A_{Pd}[H] R_{Pd}[0] \\ &- A_{Pd}[0] R_{Pd}[H]) \} \end{aligned} \quad (11)$$

It is thus found that the PPE signal generated as a result of optical absorption and optical-to-thermal power conversion depends on the Pd-electrode reflectivity difference ($R_{Pd}[0] - R_{Pd}[H]$), absorptance difference ($A_{Pd}[0] - A_{Pd}[H]$), as well as the cross terms before and after exposure to hydrogen gas, as physically expected when thermo-physical effects on boundary conditions are neglected. Through this quantity, V_t becomes a function of H_2 concentration.

Eq. (11) gives the most general case in which both metallic coatings are considered as quasi-transparent, resulting in a relatively complicated expression. In practice, we can simplify the expression by assuming a totally opaque NiAl coating, which will reduce the complexity of the boundary condition at $x = d$. In this case, the PPE signal reduces to

$$\begin{aligned} V_t(\omega, [H]) = S(\omega) \times I_1 \{ A_{NiAl} (R_{Pd}[0] - R_{Pd}[H]) \\ - (1 - A_{NiAl}) (A_{Pd}[0] - A_{Pd}[H]) \} \end{aligned} \quad (12)$$

If, furthermore, optically opaque Pd and NiAl coatings are employed on both surfaces of the PVDF film, the differential thermal PPE signal is given by the particularly simple relation

$$\begin{aligned} V_t(\omega, [H]) = S(\omega) \times I_1 (R_{Pd}[0] - R_{Pd}[H]) \\ = S(\omega) \times I_1 (A_{Pd}[0] - A_{Pd}[H]) \end{aligned} \quad (13)$$

since

$$A_{Pd} + R_{Pd} = 1.$$

In this simplest case, the thermal-related PPE signal is linearly proportional to the change of reflectivity or absorptance of the Pd coating before and after exposure to H_2 gas. Also, we find that the thermal-related PPE signal is strongest in the case both metallic coatings are opaque when compared with the quasi-transparent cases of Eqs. (11) and (12).

The third source of PPE signal is photothermal electrostatics at the Pd electrode. The origin of this source lies primarily in the shift of the Fermi level inside the Pd layer upon the filling of electronic states by electrons associated with absorbed hydrogen atoms [27]. A measurable potential difference between the front and back electrodes can appear as a result of this effect [1,26]. Another electrostatic contribution can occur due to the presence of an unbalanced electric dipole layer in the vicinity of the Pd-PVDF interface upon hydrogen absorption [26]. Therefore, the overall output PPE voltage will be the sum of the thermal and electrostatic contributions. Additional experimental work on the laser-beam modulation frequency dependence and the temperature dependence of the PPE signal from the thermal-wave interferometric sensor must be performed in order to assess the relative importance of the electrostatic components in our system. In view of the fact that the topic of this paper is the sensor performance assessment as a result of purely destructive thermal-wave interferometric operation, no attempt was made in this work to separate out these signal components. The experimental results are now discussed in terms of PPE signal phenomenology.

4. Results and discussion

4.1. Fully destructive interferometric (FDI) mode and system noise

Before the pyroelectric response on H_2 - N_2 mixtures was studied, the operation of the sensor under fully destructive PPE interferometric (FDI) mode was tested and system noise levels were identified. Fig. 3 shows the system noise level in FDI mode and the single-beam (non-interference) mode for various N_2 flow rates using the PVDF film with 53.4 nm Pd coating. The modulation frequency was 10 Hz. Fig. 3(a) shows the background electronic noise in the system, without incident radiation onto the PVDF and with no gas flow in the test cell. It can be seen that the mean noise level is $\sim 0.3 \mu V$. Fig. 3(b) shows the system noise in the presence of optical sources in the FDI mode. Two beams of intensity 4 mW each were incident on opposite surfaces of the PVDF, but there was no N_2 gas flow in the test cell. It is seen that the mean noise level increased to $\sim 0.5 \mu V$, which means that the noise induced by the laser beams (optical noise) was of the same order as the system electronic noise. Fig. 3(c) shows the system noise with two beams on in the FDI mode and N_2 gas flowing through the test cell at various flow rates. The system noise has now increased in the presence of flowing N_2 gas, as expected from the thermal nature of the pyroelectric signal generation. At the N_2 flow rate of 880 ml/min (max. flow rate available in the experiment), the noise reached $\sim 1.2 \mu V$. This noise level can thus be considered as the maximum noise floor in the FDI mode. This noise appears to be dominated by convection and

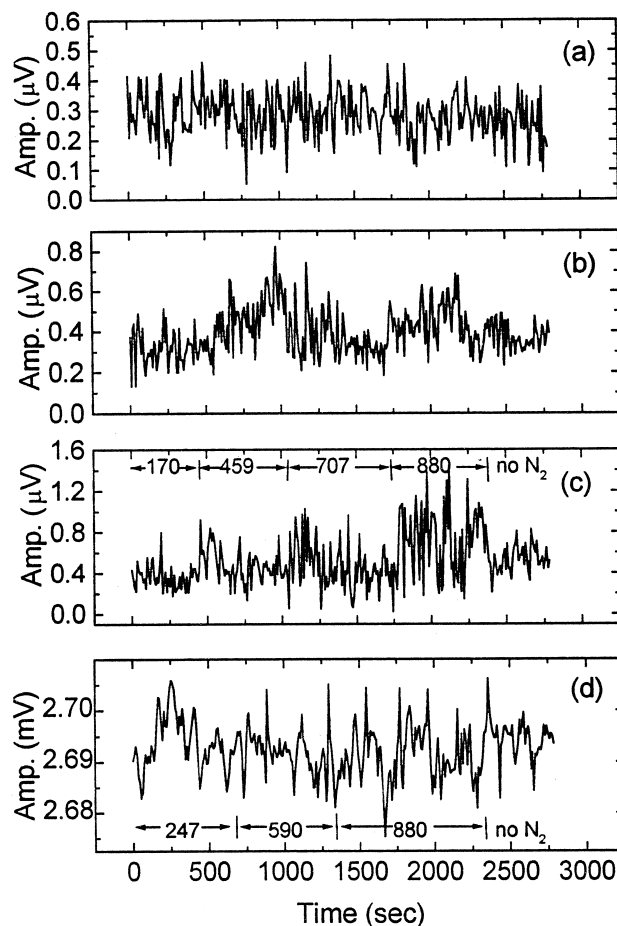


Fig. 3. PPE system noise evaluation for different operating modes. (a) system background noise without laser incidence or N_2 gas flow; (b) system noise in the FDI mode, without N_2 gas flow; (c) system noise for several N_2 flow rates in the FDI mode; (d) system noise for several N_2 flow rates in the single-beam mode. The numbers shown in (c) and (d) represent the N_2 flow rate, in ml/min.

perhaps turbulent thermal noise due to gas flow at flow rates greater than 700 ml/min. This was the rate range used for most of the experiments reported in this paper. As a comparison, Fig. 3(d) shows the noise level of the same system, under single-beam (non-interferometric) operation. It can be seen that, as expected, a large baseline signal (~ 2.7 mV) appears in the amplitude channel and the noise fluctuation is as high as $\sim 20 \mu V$, which is about 20 times that of the FDI mode. This large noise is mainly due to the uncompensated pointing noise in the single incident beam and the employment of lower instrumental sensitivity due to the large baseline signal, which tends to amplify electronic noise of all kinds. In conclusion, the real-time noise compensation in the PPE hydrogen sensor system under FDI operation improves its detectivity by approximately a factor of 20.

4.2. Signal quality as a function of Pd coating thickness

To examine and optimize the sensitivity and the response time of the sensor, the three different Pd-PVDF-

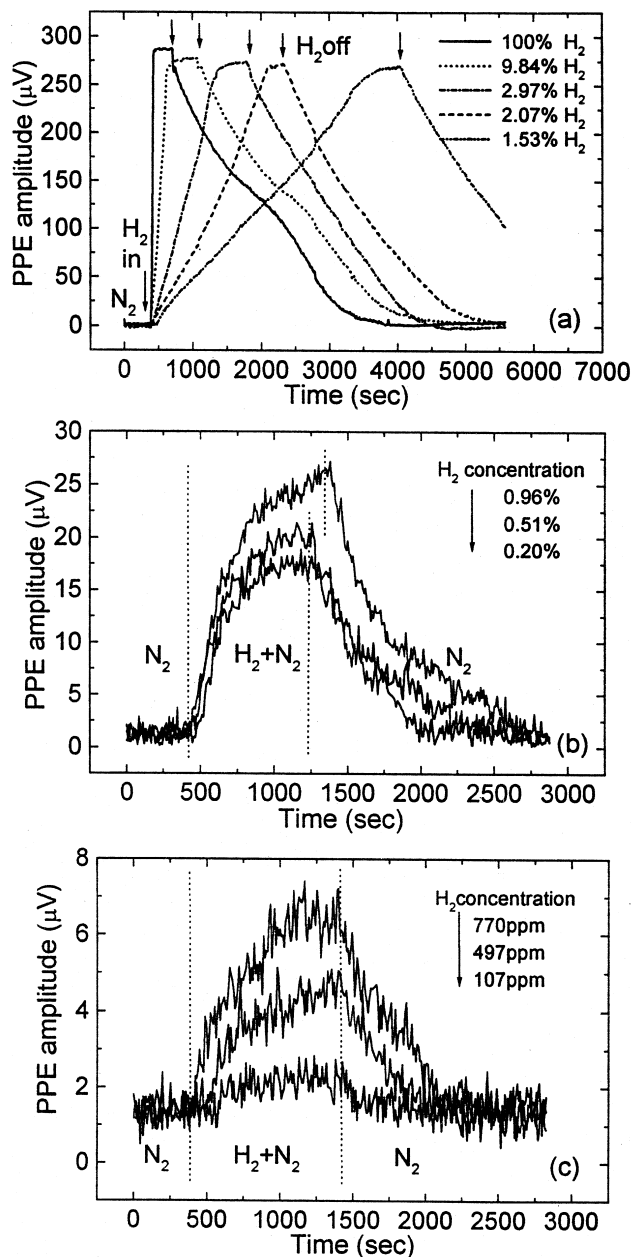


Fig. 4. PPE signal as a function of time for various concentrations of hydrogen in nitrogen using a Pd-coated (53.4 nm) PVDF film. The gas flow rate was 870 ml/min for all the experiments.

NiAl thin films described in Section 1 were used in the FDI mode. Fig. 4(a–c) show typical PPE responses as functions of time, using an active element with 53.4-nm-thick Pd, under various hydrogen concentrations in N_2 by volume. The modulation frequency was 10 Hz and the experiments were conducted at room temperature. Fig. 4(a) shows that the response time (time required for the PPE signal to rise to its maximum saturated amplitude following the introduction of H_2 in the cell) varies with H_2 concentration. The response time decreases dramatically with increasing H_2 concentration, while the signal level at saturation slightly increases with $[H_2]$. These features can be understood qualitatively, because the speed of hydrogen

adsorption on Pd and subsequent dissociation and absorption [22], and/or the speed with which the absorbed $[H]$ reaches its thermodynamic equilibrium concentration in the Pd layer, increases with increasing ambient partial pressure (concentration) of H_2 [21,22]. Furthermore, the equilibrium (saturation) $[H]$ concentration in very thin Pd films above the α - to β -phase transition [22] varies very little with ambient $[H_2]$ concentration between 1.53% and 100%. By contrast, Fig. 4(b) and (c) show what happens when the absorbed $[H]$ concentration is below the saturation concentration at equilibrium in the Pd matrix. The response time at 0.96% $[H_2]$ concentration is much shorter, and the saturated signal is much lower, than that at 1.53% $[H_2]$ concentration. This phenomenon is the result of the transition from α - to β -phase of the palladium hydride [21,22]. It can therefore be concluded that this transition occurs in the H_2 concentration of $\sim 1\%$ in N_2 by volume in the 54.3-nm Pd film. Fig. 4(c) gives the PPE output at even lower H_2 concentrations. It shows that the detection limit of the 53.4-nm Pd-coated PVDF film is about 100 ppm, which is of the same order of sensitivity as the MIS sensor [5] in which a 35 nm Pd coating was used. As a comparison, the experiments were also conducted using the same sensor, but in the single-beam mode. Fig. 5 shows the experimental results at 0.2% and 0.5% $[H_2]$. The PPE signal change due to the introduction of H_2 is almost entirely embedded in the system noise at 0.2% H_2 concentration. The detection limit of the single-beam method is thus believed to be $>0.2\%$, yielding approximately 20 times higher FDI mode detectivity, which is consistent with the system noise decrease effected by the use of PPE interferometry. The foregoing single-beam detection limit is similar to that established earlier with other single-beam optical and PPE methods [9,12,13].

Fig. 6(a–c) show the experimental results using a 25.6-nm Pd-coated PVDF thin film with various H_2 concentrations in N_2 by volume. The experiments were performed under the same conditions as in Fig. 4. Similar phenomena

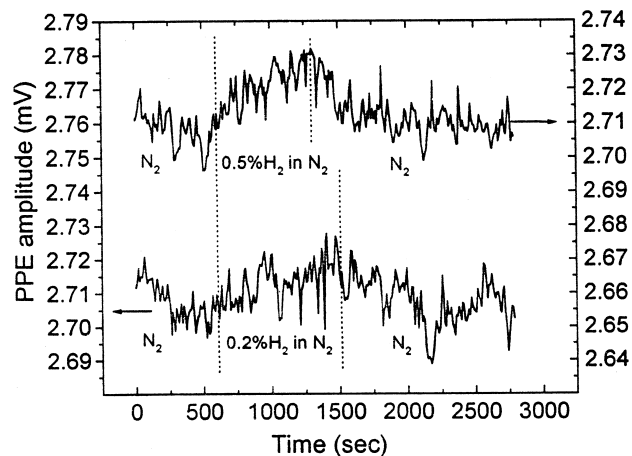


Fig. 5. PPE signal as a function of time using the single-beam method. The gas flow rate was 870 ml/min for both measurements. The two signal traces have been separated out artificially for clarity.

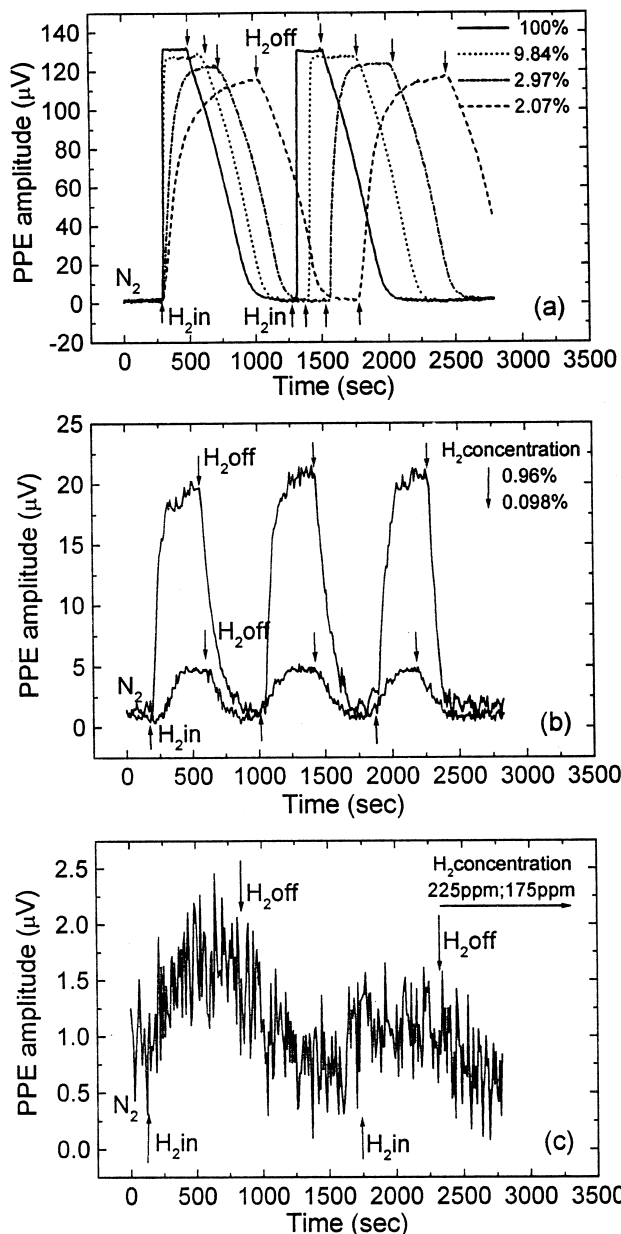


Fig. 6. PPE signal as a function of time for various concentrations of hydrogen in nitrogen using a Pd-coated (25.6 nm) PVDF film. The experimental conditions are the same as those in Fig. 4.

to Fig. 4 are observed in Fig. 6. Fig. 6(a) shows similar behavior to Fig. 4(a), with the exception of faster overall sensor response and faster onset of signal saturation. Fig. 6(b) also shows the sudden drop in response time and in saturation onset compared to the thicker Pd film in Fig. 4(b), when the sensor operates below 0.96% $[H_2]$. From Fig. 6(c) it can be estimated that the detection limit of a 25.6-nm Pd-coated PVDF sensor is in the range of 175 ppm H_2 in nitrogen, somewhat higher than with the 53.5-nm Pd film. As a comparison, the detection limit is set at approximately 0.2% $[H_2]$ concentration using the single-beam method, Fig. 7. Comparing Fig. 7 with Fig. 6, we

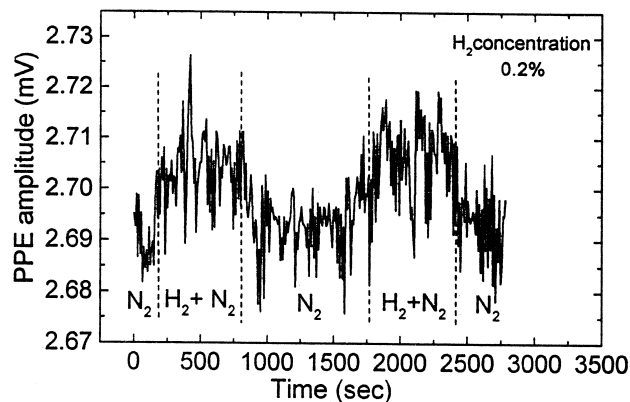


Fig. 7. PPE signal as a function of time using the single-beam method. The experimental conditions are the same as those in Fig. 6.

conclude that the signal quality at 175 ppm H_2 concentration in the FDI mode is comparable to that at 0.2% H_2 concentration in the single-beam method. Therefore, the detectivity in the FDI mode is more than 10 times higher than that of the single-beam method in the case of 25.6-nm Pd coating.

Finally, a 6.5-nm Pd-coated PVDF film was tested. Fig. 8(a) and (b) show the experimental results at various H_2

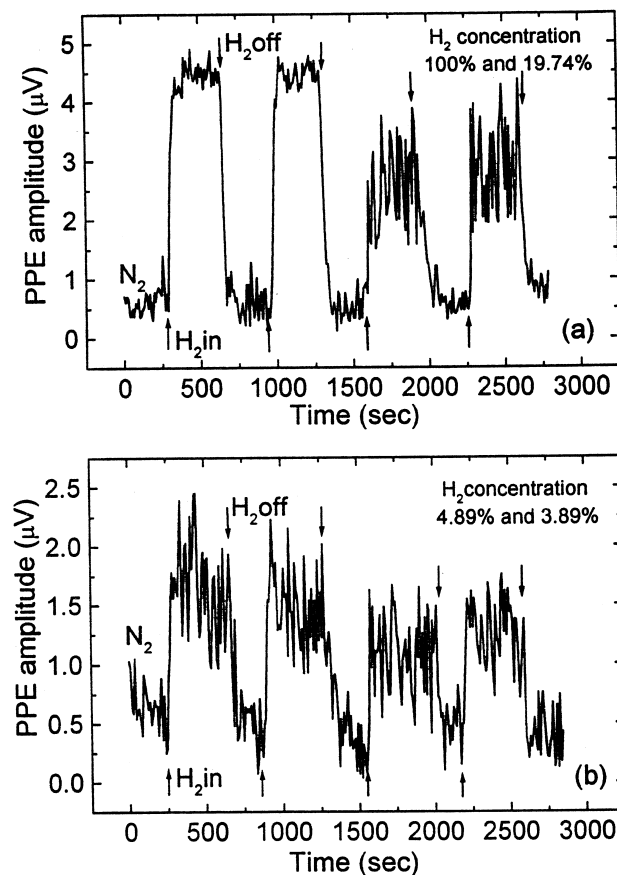


Fig. 8. PPE signal as a function of time for various H_2 concentrations in nitrogen using a Pd-coated (6.5 nm) PVDF film. The experimental conditions are the same as those used in Figs. 4 and 6.

concentrations. The experimental conditions and procedures were the same as those used in Figs. 4 and 6. Compared with those figures, Fig. 8 exhibits much lower PPE signal level, much lower sensitivity and signal-to-noise ratio, at the same H_2 concentration. The detection limit is found to be $> 2\%$ H_2 in N_2 , which is much lower than those of the thicker Pd coatings. This effect is due to the lower hydrogen retention capability by the thinnest Pd film, leading to a much lower thermodynamic equilibrium $[H]$ saturation concentration, which results in smaller changes in the optical and/or electronic properties of the film. No clear concentration region for the α -to- β -phase transition of PdH_x was found. As a comparison, the detection limit using the single-beam method under the same conditions was $> 10\%$ H_2 concentration in N_2 .

The signal-saturation-level isotherms and the response times for all three sensors with different palladium thicknesses are plotted in Fig. 9. It can be seen that the thicker Pd coatings have a narrower transition region for the α -to- β phase transformation. Unfortunately, it was not possible to clearly define the transition H_2 concentration for the thinnest Pd film in Fig. 9(a). The thicker the Pd coating, the larger the PPE output signal and subsequently the higher the device detectivity, although the difference between the PPE output signal decreases in the lower H_2

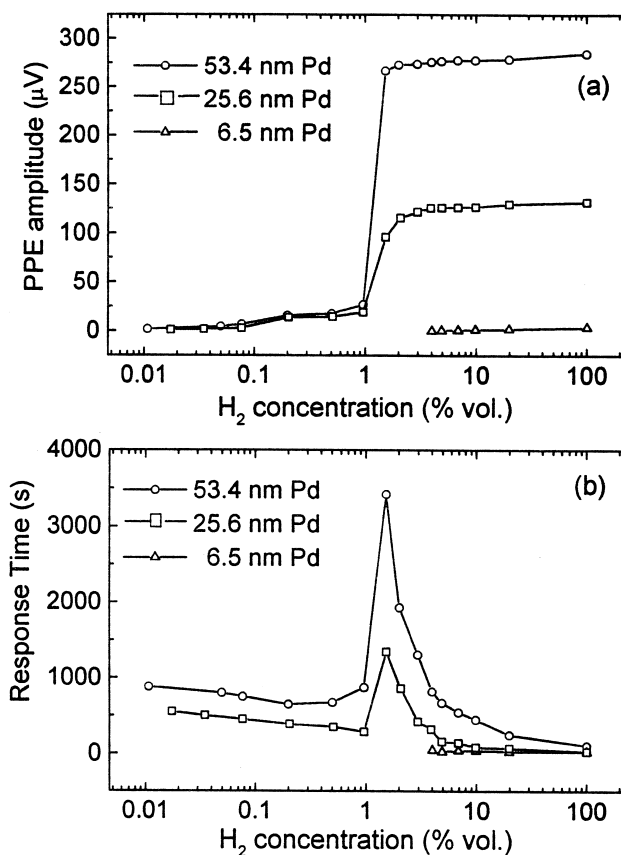


Fig. 9. (a) Measured signal-saturation-level isotherms; and (b) response times of PPE sensors with three palladium coating thicknesses.

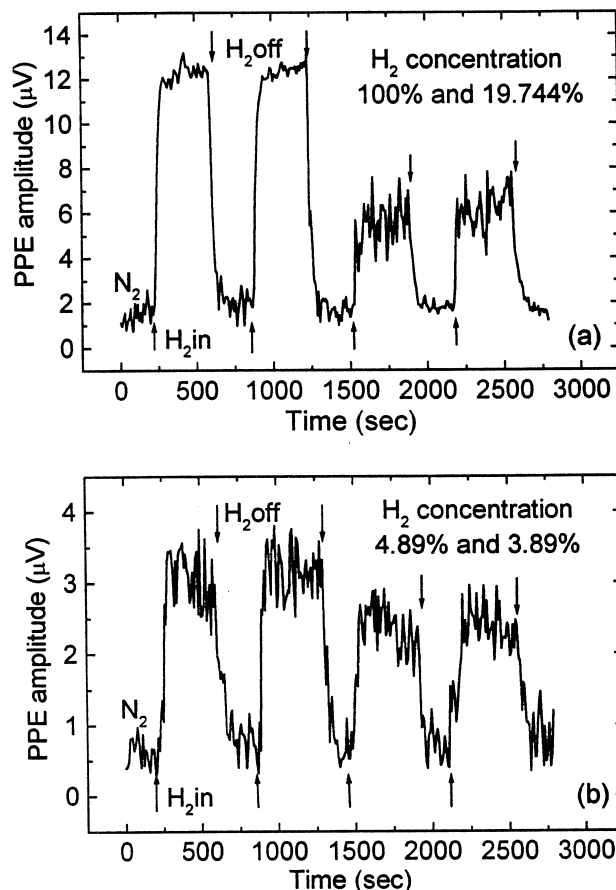


Fig. 10. PPE signal as a function of time using a 6.5-nm Pd coating on PVDF after doubling the intensity of the incident laser radiation with respect to that of Fig. 9.

concentration region ($< 1\%$). On the other hand, the thicker the Pd coating, the longer the response time, especially at H_2 hydrogen concentrations less than 10%. Noise-equivalent-power and response time are approximately anti-cor-

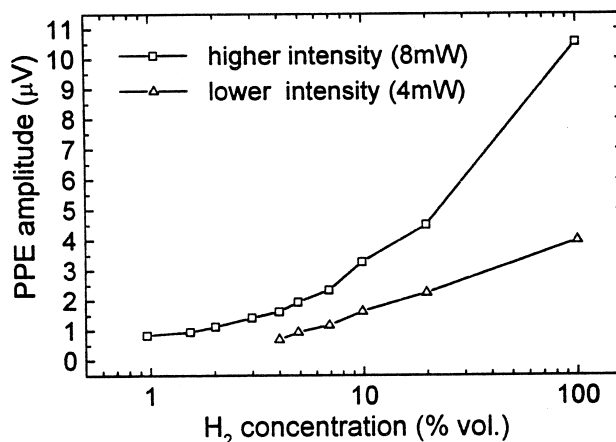


Fig. 11. Comparison of signal-saturation-level isotherms before and after doubling the laser intensity as in Fig. 10 using the 6.5-nm Pd coating on PVDF. The low-intensity experimental data are from Fig. 9(a).

related. In the present work, it was found that the optimal thickness of Pd coating is approximately 25 nm, which gives reasonably high sensitivity and short response time. The remarkable increase in response time in the neighborhood of the α -to- β transition observed in Fig. 9(b) may be related to the speed of PdH_x lattice transformation and requires further study.

4.3. Effects of incident light intensity and modulation frequency

To optimize the operation of the novel sensor system, the effects of laser radiation intensity and its modulation frequency on the PPE signal and on the detectivity were examined. For the 6.5-nm Pd-coating the experimental results at a lower intensity (4mW) are shown in Fig. 8. When the intensity was doubled, Fig. 10 shows the PPE signal and the improvement in signal-to-noise ratio. Fig. 11 gives the comparison of the PPE response as a function of ambient hydrogen concentration in nitrogen for these two intensities. It is seen that the PPE signal amplitude is approximately double at the double intensity, within experimental error. This result is consistent with the theoretical prediction of linear dependence on I_1 in Eq. (10). Moreover, as a result of increasing the signal level and, there-

fore, the signal-to-noise ratio (compare Figs. 8 and 10), the detectivity was improved by two to three times.

Since the PPE signal is a function of the laser-intensity modulation frequency, it is important to select an optimal operating frequency for the sensor. Fig. 12 shows the PPE signal at two different modulation frequencies, $f = 10$ Hz and 26.1 Hz, using the 25.6-nm Pd PVDF detector at two H_2 concentrations. It is demonstrated that the amplitude of the PPE signal decreases rapidly with increasing frequency, which is consistent with Eq. (7), and is borne out by the PPE theory [19,20,25]. In electronic systems such as the present PPE sensor, $1/f$ noise becomes an important noise source at low frequencies [28]. This suggests that operation at relatively high frequencies would be desirable. However, $1/f$ noise is not the dominant noise source at the modulation frequency of 10 Hz for the present system. Dominant noise sources are mainly the thermal fluctuations due to gas flow and possibly turbulence, and laser pointing noise as discussed in Section 4.1. As a result, one cannot reduce the overall noise level by increasing the modulation frequency, with the concomitant decrease of PPE amplitude, which also results in a rapid decline of signal-to-noise ratio. In the present work, the operating frequency was thus selected to be 10 Hz: at this frequency one may obtain an optimally large PPE signal, which does not become dominated by $1/f$ noise.

5. Conclusions

In this work, a simple and sensitive solid-state sensor for trace H_2 detection based on PPE thermal-wave interferometry has been developed. The phenomenological mechanism of signal generation, the operating characteristics of the sensor, and the quantitative phenomenology of the sensor response have been investigated. The experimental results demonstrated much improved detectivity and enhanced signal dynamic range over our earlier single-ended PPE hydrogen sensors [1], due to the coherent suppression of the baseline signal and (at least partial) suppression of laser pointing noise. This is the first attempt to exploit the fully destructive thermal-wave interference within a single pyroelectric thin film for chemical sensor applications. The main conclusions of our studies are summarized below.

(1) The employment of fully destructive thermal-wave interference within a PVDF element makes this sensor highly sensitive with a very wide detection dynamic range between 100% and 100 ppm of $[\text{H}_2]$ in N_2 . Unlike conventional signal normalization through ratioing by a reference signal, this technique utilizes the real-time laser-beam fluctuation compensation effected by the subtraction of PPE signal amplitudes generated at the front and the back of the active element. This scheme avoids noise addition from independent amplifiers used to amplify and ratio

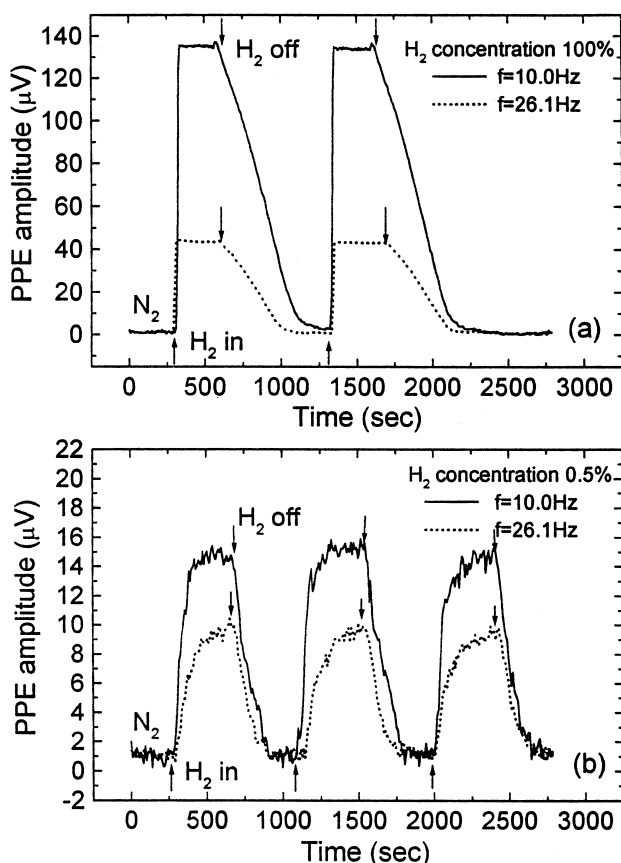


Fig. 12. Frequency dependence of the PPE signal using a PPE sensor with a 25.6-nm Pd coating and two H_2 concentrations: (a) 100%; (b) 0.5%.

between two independent signals. The detector was found to be reversible and durable. The experiment has shown a reversible response for several hundred exposures to H₂ with no Pd blistering or peel-off effects.

(2) Based on fully destructive thermal-wave interferometry within a PVDF film detector, extensions of the present measurements to the detection of other environmentally important gases or vapors is very promising. This technique is also expected to have potential applications in surface science, specifically in the further understanding of hydrogen adsorption/absorption in ultra-thin Pd films on pyroelectric substrates [29].

Acknowledgements

The support of the Natural Sciences and Engineering Research Council of Canada (NSERC) through a Research Grant is gratefully acknowledged.

References

- [1] A. Mandelis, C. Christofides, *Physics, Chemistry, and Technology of Solid State Gas Sensor Devices*, Chemical Analysis Vol. 125, in: J.D. Winefordner (Ed.), Wiley, New York, 1993.
- [2] K.I. Lundstrom, M.S. Shivaraman, C.M. Svensson, A hydrogen-sensitive Pd-gate MOS transistor, *J. Appl. Phys.* 46 (1975) 3876–3881.
- [3] K.I. Lundstrom, M.S. Shivaraman, C.M. Svensson, Chemical reaction on Palladium surfaces studied with Pd-MOS structures, *Surf. Sci.* 64 (1977) 497.
- [4] M.C. Steele, B.A. MacIver, Palladium/cadmium-sulfide Schottky diode for hydrogen detection, *Appl. Phys. Lett.* 28 (1976) 687–688.
- [5] A. D'Amico, G. Fortunato, G. Petrocco, Transport properties of Pd/insulator/a-Si:H Schottky diode for hydrogen detection, *Sensors and Actuators* 4 (1983) 34.
- [6] T. Yamamoto, M. Morimoto, Thin-MIS-structure Si negative-resistance diode, *Appl. Phys. Lett.* 20 (1976) 269–270.
- [7] T.L. Poteat, B. Lalevic, Transition metal-gate MOS gaseous detectors, *IEEE Trans. Electron Devices* ED-29 (1982) 123–129.
- [8] A. D'Amico, A. Palma, E. Verona, Palladium-surface acoustic wave interaction for hydrogen detection, *Appl. Phys. Lett.* 41 (1982) 300–301.
- [9] M.A. Butler, Micromirror optical-fiber hydrogen sensor, *Sensors and Actuators B* 22 (1994) 155–163.
- [10] A. Bearzotti, C. Caliendo, E. Verona, A. D'Amico, Integrated optical sensor for the detection of H₂ concentrations, *Sensors and Actuators B* 7 (1992) 685–688.
- [11] A. Mandelis, C. Christofides, Photopyroelectric (P²E) sensor for trace hydrogen gas detection, *Sensors and Actuators B* 2 (1990) 79–87.
- [12] A. Mandelis, J.A. Garcia, Pd/PVDF thin film hydrogen sensor based on laser-amplitude-modulated optical-transmittance: dependence on H₂ concentration and device physics, *Sensors and Actuators B* 49 (1998) 258–267.
- [13] J.A. Garcia, A. Mandelis, Study of the thin-film palladium/hydrogen system by an optical transmittance method, *Rev. Sci. Instrum.* 67 (1996) 3981–3983.
- [14] R. Wagner, A. Mandelis, Separation of thermal-wave and optical reflectance effects in Palladium-photopyroelectric hydrogen sensors, *Ferroelectrics* 165 (1995) 193–203.
- [15] C. Christofides, A. Mandelis, J. Rawski, S. Rehm, Photopyroelectric detection of hydrogen/oxygen mixtures, *Rev. Sci. Instrum.* 64 (1993) 3563–3571.
- [16] Y. Oh, J. Hamagami, Y. Watanabe, M. Tanaka, H. Yanagida, A novel palladium thin film hydrogen-detector, *J. Ceram. Soc. Jpn.* 110 (1993) 618–620.
- [17] S.Y. Choi, K. Takahashi, M. Esashi, T. Matsuo, Stabilization of MISFET hydrogen sensors, *Sensors and Actuators* 9 (1986) 353–361.
- [18] M. Armgarth, C. Nylander, Blister formation in Pd gate MIS hydrogen sensors, *IEEE Electron Dev. Lett.* EDL-3 (1982) 384–386.
- [19] C.-H. Wang, A. Mandelis, Purely-thermal wave interferometry, *J. Appl. Phys.* (in press).
- [20] C.-H. Wang, A. Mandelis, Measurement of Thermal Diffusivity of air using photopyroelectric interferometry, *Rev. Sci. Instrum.* (in press).
- [21] K. Wyrzykoski, A. Rodzik, B. Baranowski, Optical transmission and reflection of PdH_x thin films, *J. Condens. Matter* 1 (1989) 2269–2277.
- [22] F.A. Lewis, *The Palladium/Hydrogen System*, Academic, New York, 1967, pp. 1–12.
- [23] K. von Rottkay, M. Rubin, Refractive index changes of Pd-coated magnesium lanthanide switchable mirrors upon hydrogen insertion, *J. Appl. Phys.* 85 (1999) 408–413.
- [24] KYNAR Piezo Film Technical Manual, Pennwalt, King of Prussia, PA, 1983.
- [25] A. Mandelis, M. Zver, Theory of the photopyroelectric effect in solids, *J. Appl. Phys.* 57 (1985) 4421–4430.
- [26] A. Mandelis, C. Christofides, Photothermal electrostatics of the Pd-PVDF photopyroelectric (PPE) hydrogen gas sensor, *J. Appl. Phys.* 70 (1991) 4496–4505.
- [27] G. Fortunato, A. Bearzotti, C. Caliendo, A. D'Amico, Hydrogen sensitivity of Pd/SiO₂/Si structure: a correlation with the hydrogen-induced modifications on optical and transport properties of α -phase Pd film, *Sensors Actuators* 16 (1989) 43.
- [28] Van der Ziel, *Noise in Measurement*, Wiley, New York, 1976, p. 160.
- [29] Y. Fukai, *The Metal-Hydrogen System: Basic Bulk Properties*, Springer-Verlag, New York, 1993.